Optical intersubband absorption of coupled double quantum wells embedded in an asymmetric Fabry-Perot microcavity subjected to an electric field

1998 J. Phys.: Condens. Matter 10 3285

(http://iopscience.iop.org/0953-8984/10/14/017)

J. Phys.: Condens. Matter **10** (1998) 3285–3292. Printed in the UK PII: S0953-8984(98)90289-2

Optical intersubband absorption of coupled double quantum wells embedded in an asymmetric Fabry–Perot microcavity subjected to an electric field

Xin Chen†§ and Mufei Xiao‡

† Department of Electronics, University of York, York YO1 5DD, UK

‡ Centre for Condensed Matter Sciences–UNAM, PO Box 2681, CP-22800 Ensenada, Mexico

Received 5 January 1998, in final form 5 February 1998

Abstract. On the basis of a local-field theory, the field in a quantum-well microcavity structure is rigorously derived, and the expression for the optical absorption is given. Then, the optical absorption in coupled double quantum wells ($Al_xGa_{1-x}As/GaAs$) embedded in an asymmetric microcavity is studied. The influences of different parameters of the quantum-well microcavity and applied field strengths on the intersubband absorption are discussed.

1. Introduction

Recently the optical properties of quantum-well structures embedded in a microcavity have attracted a lot of interest for both fundamental physics and application reasons [1–12], since in such a structure the electrons and field are both confined in one direction, by the quantum well and the cavity, respectively. This thus allows us to carry out a study of the light–matter interaction in such a manner that by detuning the coupling between the quantum wells and the modes of the optical field supported by the microcavity, one can effectively control the light–quantum-well interaction [1, 2]. Different theoretical approaches have been used to study the quantum-well microcavity systems [3–8]. Also, investigations of the second-harmonic generation from a vertical cavity [9, 10] and bistability [11] in a microcavity have been carried out. For a detailed review, the reader is referred to reference [12].

In the last decade, the local-field effects on optical properties of quantum-well structures have been studied [13–19]. It has been demonstrated that, to obtain an accurate prediction of the optical properties of normal quantum-well structures, it is necessary to include the local-field effects [13]. In this paper we use a local-field theory to investigate the linear optical absorption of coupled double quantum wells embedded in an asymmetric microcavity under the influence of an external electric field.

This paper is organized as follows. In section 2, starting from the Maxwell–Lorentz equations, the expression for the field in each layer is given, and the field in the quantum wells is determined via an integral equation. Then, by matching the boundary conditions, the field in the quantum-well microcavity structure is determined, and the field determined is used to calculate the absorption. In section 3, on the basis of the theory developed in the previous section, detailed numerical calculations for different parameters of the microcavity and field strengths are performed, and the influences of the fineness of the microcavity and the field strength on the intersubband absorption are shown.

§ Fax: +44 1904 432335; telephone: +44 1904 430000-2407; e-mail: xc2@york.ac.uk.

0953-8984/98/143285+08$19.50

2. Theoretical framework

The basic structure under consideration is constructed from three layers (a/b/c) which are characterized by their dielectric constants:

$$\epsilon(z) = \begin{cases} \epsilon_a & z < 0, \text{ layer a} \\ \epsilon_b & 0 < z < L, \text{ layer b} \\ \epsilon_c & z > L, \text{ layer c} \end{cases} \tag{1}$$

and coupled double quantum wells are placed in layer b, which is located at L_1; the well widths are d_1 and d_2, respectively, and the width of the barrier is d_b. In order to construct the Fabry–Perot microcavity, two stacks of distributed Bragg reflecting layers (DBR) are placed in front of and behind the basic cavity of length L. F is the applied electric field (cf. figure 1).

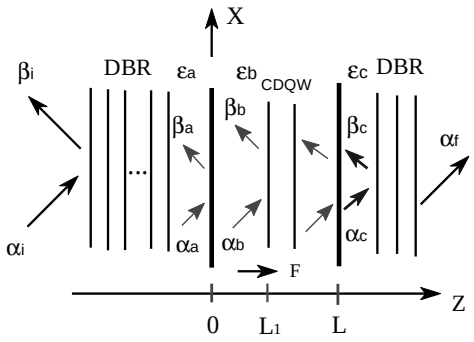

Figure 1. A schematic view of the quantum-well microcavity structure. α_i is the amplitude of the incident field before the first DBR; α_a is the amplitude of the field in the layer just outside the cavity (behind the first DBR); α_b is the amplitude of the field incident on the quantum wells; α_c is the amplitude of the field just outside the cavity (behind the cavity); α_f is the amplitude of the transmitted field behind the second DBR. β_j is the corresponding reflected field. F is the applied field.

Since only a p-polarized incident field is applied, it is sufficient to consider the x- and z-components of the field. Let us first consider the basic cavity structure, and cope with the DBR later. According the Maxwell–Lorentz equations, the electric field in each layer is determined by the wave equations, and the electric field has the following form:

$$\boldsymbol{E}_j(z) = (\alpha_j \mathrm{e}^{\mathrm{i}q_\perp^{(j)}z} + \beta_j \mathrm{e}^{-\mathrm{i}q_\perp^{(j)}z})\boldsymbol{e}_x - \frac{q_\parallel}{q_\perp^{(j)}}(\alpha_j \mathrm{e}^{\mathrm{i}q_\perp^{(j)}z} - \beta_j \mathrm{e}^{-\mathrm{i}q_\perp^{(j)}z})\boldsymbol{e}_z \qquad \text{in layer } j = \text{a or c} \tag{2}$$

and due to the presence of the quantum well the field in layer b is modified by [14–16]

$$\boldsymbol{E}_B(z) = \boldsymbol{E}_b(z) - \mathrm{i}\mu_0\omega \int\int \mathbf{G}(z - z')\boldsymbol{\sigma}(z', z'')\boldsymbol{E}_B(z'')\ \mathrm{d}z''\ \mathrm{d}z' \tag{3}$$

where the background field, $\boldsymbol{E}_b(z)$, is the field with no quantum well embedded in the layer b, which is given by equation (2). $\mathbf{G}(z-z')$ is the appropriate propagator [13] and $\boldsymbol{\sigma}(z', z'')$ is the linear conductivity tensor of the well. We assume that in the quantum well there are only two confined states in the conduction band, which is a good approximation when the incident photon energy is close to the energy separation considered, of which only the lower

state is populated by electrons. In this case, as derived from the density-matrix approach, the linear conductivity tensor takes a diagonal form [13].

The tensor forms of the propagator and the conductivity allow us to rewrite equation (3) in matrix notation:

$$\boldsymbol{E}_B(z) = \boldsymbol{E}^b(z) + \boldsymbol{\Xi}(z)\boldsymbol{\gamma} \tag{4}$$

where

$$\boldsymbol{\Xi}(z) = \left[\int \mathbf{G}(z-z')\mathbf{T}(z')\ \mathrm{d}z'\right]\boldsymbol{\zeta} \tag{5}$$

$$\boldsymbol{\gamma} = \int \mathbf{T}(z'')\boldsymbol{E}_B(z'')\ \mathrm{d}z''. \tag{6}$$

The explicit expressions for $\mathbf{T}(z'')$ and $\boldsymbol{\zeta}$ are given in the appendix.

For the present, we focus on the z-component of the local field in the layer b, since the x-component is slowly varying across the well [13]. By multiplying the z-part of the local field (equation (4)) by $\Phi(z)$ and thereafter integrating the resultant equation, one immediately realizes that the parameters γ_z are determined via

$$\gamma_z = -\frac{q_\parallel}{q_\perp^{(b)}}\frac{\alpha_b - \beta_b}{1 - S_{zz}}\int \Phi(z)\ \mathrm{d}z \tag{7}$$

where

$$\begin{aligned} S_{zz} &= \int \Phi(z)\Xi_{zz}(z)\ \mathrm{d}z\ \zeta_{zz} \\ &= \left(\frac{c_0}{\omega}\right)^2 \frac{1}{\epsilon_b}\left\{\int \Phi^2(z)\ \mathrm{d}z + \frac{q_\parallel^2}{2\mathrm{i}q_\perp}\left[\int \Phi(z)\int \mathrm{e}^{\mathrm{i}q_\perp^{(b)}|z-z'|}\Phi(z')\ \mathrm{d}z'\ \mathrm{d}z\right]\right\}\zeta_{zz}. \end{aligned} \tag{8}$$

Before going further, we make the assumption that the DBR behind the basic cavity is removed, since the light is totally reflected at the interface b/c, which will be considered later; thus $\alpha_c = \alpha_f$ and $\beta_c = 0$. In order to determine the as-yet unknown α_b and β_b, one has to match the boundary conditions, namely, the continuities of $E_x(z)$ and $D_z(z)$ at the interfaces, $z = 0$ and $z = L$. Thereafter, eliminating α_c and β_a in favour of α_b and β_b, then inserting α_b and β_b into equation (7), one finally obtains

$$\gamma_z = \frac{\kappa}{1+\Gamma} \tag{9}$$

where

$$\begin{aligned} \Gamma = &\left[\left(\int \Phi(z)\ \mathrm{d}z\ q_\parallel\right)\Big/\left[(1 + r_{ab}r_{bc}\mathrm{e}^{2\mathrm{i}q_\perp^{(b)}L})q_\perp^{(b)}\right]\right] \\ &\times \left[r_{ab}(1 + r_{bc}\mathrm{e}^{2\mathrm{i}q_\perp^{(b)}L})\Xi_{xz}(0) + t_{ab}r_{bc}\mathrm{e}^{\mathrm{i}q_\perp^{(b)}L}\Xi_{xz}(L)\right] - S_{zz} \end{aligned} \tag{10}$$

and

$$\kappa = -\frac{\alpha_a t_{ab} q_\parallel (1 + r_{bc}\mathrm{e}^{2\mathrm{i}q_\perp^{(b)}L})}{(1 + r_{ab}r_{bc}\mathrm{e}^{2\mathrm{i}q_\perp^{(b)}L})q_\perp^{(b)}}\int \Phi(z)\ \mathrm{d}z \tag{11}$$

where r_{ab} and r_{bc} are the amplitude reflection coefficients at the interfaces a/b and b/c, respectively, and $t_{ab} = 1 - r_{ab}$.

Having determined the local field in the quantum-well microcavity system, and according to the definition of the Fresnel reflection coefficient (R_p), one has

$$R_p = -\frac{\beta_a}{\alpha_a} = r_p - \frac{1 + r_{ab}}{1 + r_{ab} r_{bc} \mathrm{e}^{2\mathrm{i}q_\perp^{(b)} L}} \left[\Xi_{xz}(0) - r_{bc} \mathrm{e}^{\mathrm{i}q_\perp^{(b)} L} \Xi_{xz}(L) \right] \gamma_z \tag{12}$$

where r^p is the reflection coefficient in the absence of the well, which is also given in the appendix.

In the absence of the quantum well, the equations derived above return to the form for a standard three-layer structure, as expected. The effects of DBR can be easily included in our theory via a transfer-matrix approach after determining the local field. The amplitudes of the incoming field and the field after the DBR can be determined via the relation [20]

$$\begin{pmatrix} \alpha_i \\ \beta_i \end{pmatrix} = \mathbf{M}^N \begin{pmatrix} \alpha_a \\ \beta_a \end{pmatrix} = \mathbf{M}_n \begin{pmatrix} \alpha_a \\ \beta_a \end{pmatrix} \tag{13}$$

where $\mathbf{M}$ is the 2×2 transfer matrix, and N is the number of paired layers constructing the DBR. One can easily find that

$$r = -\frac{\beta_i}{\alpha_i} = \frac{M_n(2,2) R_p - M_n(2,1)}{M_n(1,1) - M_n(1,2) R_p}. \tag{14}$$

It can be seen from equation (14) that without DBR in front of the cavity, i.e. with $\mathbf{M}_n = \mathbf{1}$, we have $\alpha_i = \alpha_a$ and $r = R_p$, as expected.

Since the light is totally reflected at the interface b/c, the absorption A_p is determined via

$$A_p = 1 - |r|^2 = 1 - \left| \frac{M_n(2,2) R_p - M_n(2,1)}{M_n(1,1) - M_n(1,2) R_p} \right|^2. \tag{15}$$

3. Numerical results and discussion

In this section we present detailed numerical calculations for the linear optical absorption arising from intersubband transitions. The parameters used in the calculations are given as follows: the widths of the chosen $Al_{0.3}Ga_{0.7}As/GaAs$ quantum wells are $d_1 = 30$ Å, $d_b = 30$ Å and $d_2 = 40$ Å, and the normalizing factor $\omega_{21} = \varepsilon_{21}/\hbar$. The coupled double quantum wells are located symmetrically in the cavity for all of the cases. The dielectric constants of layers b and c are $\epsilon_b = 13.1$, $\epsilon_c = 1.0$, and the length of the cavity is 0.5 μm. The materials constructing the front DBR layers are GaAs and $Al_{0.67}Ga_{0.63}As$, and thus the dielectric constants are 13.1 and 11.0, respectively. The angle of incidence is 60° and $\hbar/\tau = 3$ meV.

Figure 2 shows the absorption as a function of normalized incoming frequency for different paired DBR layers added to the basic cavity. The n-doping density is 0.7×10^{12} cm^{-2}. It appears from figure 2 that as only one pair of DBR layers is added to the cavity the absorption spectrum shows only one peak, which is located at $\sim 1.13\omega_{21}$ due to the local-field corrections [14–16]. However, the absorption spectrum still shows an asymmetric shape due to the cavity effects. With three paired DBR layers placed in front of the cavity the amplitude of the absorption decreases, the peak is slightly red-shifted and the spectrum becomes broadened. When five DBR layers are added to the cavity, the peak at $\sim 1.13\omega_{21}$ keeps decreasing and being broadened, and the peak is blue-shifted. We begin to see that a shoulder develops close to ω_{21}. When seven paired DBR layers are added to the cavity, the peak above $1.1\omega_{21}$ is blue-shifted and becomes narrower, and the peak is also increased in magnitude; the shoulder becomes a distinct peak. When ten paired

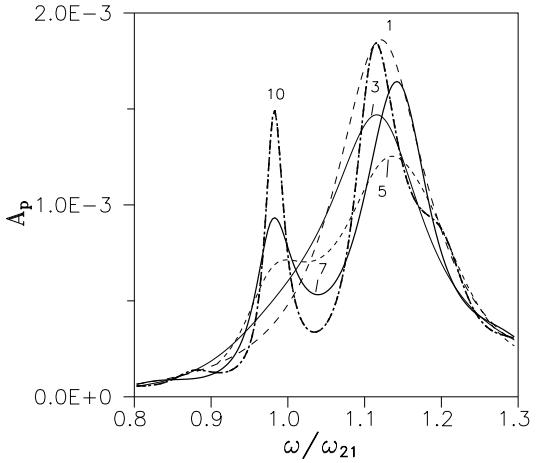

Figure 2. The absorption as a function of the normalized frequency for different paired DBR layers added to the basic cavity.

DBR layers are added to the cavity, the two peaks at $\sim 0.97\omega_{21}$ and $\sim 1.13\omega_{21}$ become even narrower, and both peaks are increased in magnitude; of the increases, that of the peak at $\sim 0.97\omega_{21}$ is larger than that of the other peak. One may also notice that a shoulder develops at $\sim 1.2\omega_{21}$ and a peak appears at $\sim 0.87\omega_{21}$. From the five curves presented in figure 2, we can see that with more and more DBR layers added to the cavity the peak located somewhat above $1.1\omega_{21}$ first becomes decreased and broadened, then, together with additional peak(s) appearing close to ω_{21}, the peak starts to become sharper and bigger; the peak above $1.1\omega_{21}$ can be red-shifted or blue-shifted. Since this peak is due to the resonance of γ_z, with the change of the fineness of the cavity the resonance condition for γ_z is also modified. Due to the high fineness of the cavity, the interaction between the light supported by the cavity and the quantum wells is enhanced and as a result additional peaks appear at $\omega \lesssim \omega_{21}$.

Figure 3 shows the absorption as a function of the normalized frequency for different

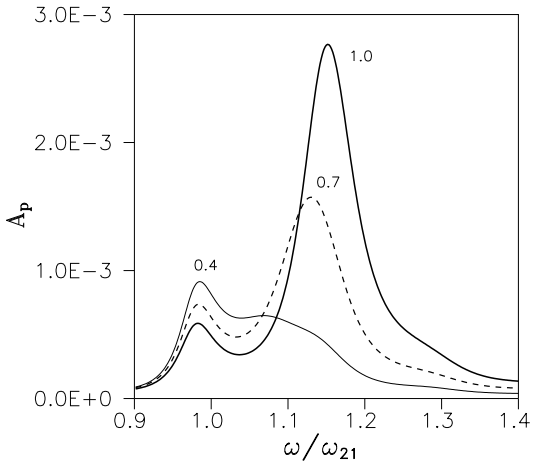

Figure 3. The absorption as a function of the normalized frequency for different doping densities (as indicated, $\times 10^{12}$ cm^{-2}). There are seven DBR layers placed in front of the cavity.

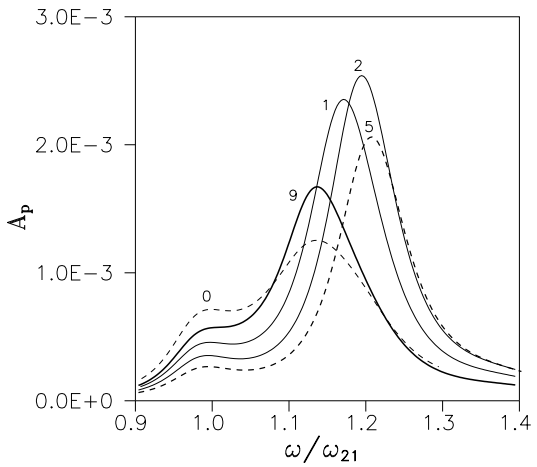

Figure 4. The absorption as a function of the normalized frequency for different electric field strengths as indicated (in V μm^{-1}). There are five DBR layers placed in front of the cavity.

doping densities (as indicated, $\times 10^{12}$ cm^{-2}). There are seven DBR layers placed in front of the cavity. It can be seen from figure 3 that when the doping density is 0.4×10^{12} cm^{-2}, the peak above ω_{21} is very broadened, while the peak due to the interaction between the cavity and the quantum wells is quite clear; as the doping density increases to 0.7×10^{12} cm^{-2}, the peak above ω_{21} becomes distinct and its amplitude increases, while the peak below ω_{21} is reduced in magnitude and the splitting between the two peaks increases owing to the blue-shift of the peak above ω_{21}; when the doping increases up to 1.0×10^{12} cm^{-2} the tendency becomes clearer. It is clear that as the doping density is changed, the resonance condition for γ_z is also changed due to the change of the condition tensor. With increase of the doping density, the shift and the increase of the peak above ω_{21} have been observed in the usual quantum-well systems [15]. The peak due to the strong interaction between the cavity and the quantum wells remains at $\sim 0.97\omega_{21}$. However, the amplitude of this peak is reduced with the increase of the doping density.

Finally we study the behaviour of the linear optical absorption of the coupled double quantum wells under the influence of the applied electric field. Figure 4 shows the absorption as a function of the normalized frequency for different electric field strengths as indicated (in V μm^{-1}). The n-doping density is 0.7×10^{12} cm^{-2}, and there are five DBR layers placed in front of the cavity. It appears from figure 4 that with the variation of the applied electric field strength, the peak above $1.1\omega_{21}$ moves in the range $1.1\omega_{21} \lesssim \omega \lesssim 1.25\omega_{21}$. From numerical calculations we know that, as the field strength is close to 5 V μm^{-1}, the wavefunctions of the ground and excited states dwell evenly in both narrow and wide wells—that is, it is in the resonant tunnelling stage [19] that the peak is located at $\sim 1.25\omega_{21}$; this also implies that at this field strength the splitting of the two peaks reaches its maximum, since the peak below ω_{21} remains at $\sim 0.97\omega_{21}$. Also at this field strength, the peak below ω_{21} reaches its minimum in magnitude. With a further increase of the field strength the peak above $1.1\omega_{21}$ begins to be red-shifted, and when the field strength is set to 9.0 V μm^{-1} this peak moves back to the position it had for $F = 0$. It is worth pointing out that, without inclusion of the local-field effects, the peak on the high-frequency side will locate exactly at ω_{21} for different applied field strengths, which can be easily seen by setting $\gamma_z = \int \Phi(z) E_{b,z}(z)\, \mathrm{d}z$.

In conclusion, in this paper we have used the local-field theory to study the optical

intersubband absorption of coupled double quantum wells embedded in an asymmetric microcavity. Numerical results show that changing of the fineness of the microcavity, the doping density and applied field strength can lead to significant modification of the intersubband absorption of the wells in the cavity.

Appendix

In this part we give detailed definitions of some of the parameters used in the main part of the paper.

The linear conductivity tensor entering equation (3) takes a diagonal form and the relevant non-zero components of the conductivity tensor are given via [14]

$$\sigma_{xx}(z', z'') = \frac{\mathrm{i}e_0^2}{2\pi\hbar^2\omega}\frac{(\varepsilon_2-\varepsilon_1)(\varepsilon_F-\varepsilon_1)^2}{[\hbar(\omega+\mathrm{i}/\tau)]^2-(\varepsilon_2-\varepsilon_1)^2}\phi(z')\phi(z'') \tag{A.1}$$

$$\sigma_{zz}(z', z'') = \frac{\mathrm{i}e_0^2}{2\pi m\omega}\frac{(\varepsilon_2-\varepsilon_1)(\varepsilon_F-\varepsilon_1)}{[\hbar(\omega+\mathrm{i}/\tau)]^2-(\varepsilon_2-\varepsilon_1)^2}\Phi(z')\Phi(z'') \tag{A.2}$$

and two abbreviations are introduced:

$$\phi(z) = \psi_1(z)\psi_2(z) \qquad \Phi(z) = \psi_1(z)\frac{\mathrm{d}\psi_2(z)}{\mathrm{d}z} - \psi_2(z)\frac{\mathrm{d}\psi_1(z)}{\mathrm{d}z}. \tag{A.3}$$

In the equations above, e_0 is the electron charge, m denotes the effective mass and τ is the relaxation time associated with intersubband transitions. ε_2 and ε_1 are the ground- and excited-state energies, and $\psi_2(z)$ and $\psi_1(z)$ are the ground- and excited-state wavefunctions, respectively. The global charge-neutrality condition has been used in the determination of the Fermi energy, ε_F.

In equation (5), $\mathbf{T}(z)$ and $\boldsymbol{\zeta}$ are given by

$$\mathbf{T}(z) = \begin{pmatrix} \phi(z) & 0 \\ 0 & \Phi(z) \end{pmatrix} \tag{A.4}$$

$$\boldsymbol{\zeta} = \begin{pmatrix} \zeta_{xx} & 0 \\ 0 & \zeta_{zz} \end{pmatrix} \tag{A.5}$$

and the non-zero elements of $\boldsymbol{\zeta}$ are given by

$$\zeta_{xx} = \frac{\mu_0 e_0^2}{\pi\hbar^2}\frac{(\varepsilon_2-\varepsilon_1)(\varepsilon_F-\varepsilon_1)^2}{[\hbar(\omega+\mathrm{i}/\tau)]^2-(\varepsilon_2-\varepsilon_1)^2} \tag{A.6}$$

$$\zeta_{zz} = \frac{\mu_0 e_0^2}{2\pi m}\frac{(\varepsilon_2-\varepsilon_1)(\varepsilon_F-\varepsilon_1)}{[\hbar(\omega+\mathrm{i}/\tau)]^2-(\varepsilon_2-\varepsilon_1)^2}. \tag{A.7}$$

In equation (12), r^p is the reflection coefficient in the absence of the wells, which is given by

$$r_p = \frac{r_{ab} + r_{bc}\mathrm{e}^{2\mathrm{i}q_\perp^{(b)}L}}{1 + r_{ab}r_{bc}\mathrm{e}^{2\mathrm{i}q_\perp^{(b)}L}}. \tag{A.8}$$

References

[1] Weisbuch C, Nishioka M, Ishikawa A and Arakawa Y 1992 *Phys. Rev. Lett.* **69** 3314

[2] Citrin D S 1994 *IEEE J Quantum Electron.* **30** 977 and references therein

[3] Panzarini G and Andreani L C 1995 *Phys. Rev.* B **52** 10 780

[4] Ivchenko E L, Kaliteevski M A, Kavokin A V and Nesvizhskii A I 1996 *J. Opt. Soc. Am.* B **13** 1061 and references therein

[5] Jorda S 1995 *Phys. Rev.* B **51** 10 185
Jorda S 1996 *Solid State Commun.* **97** 7
Jorda S 1996 *J. Opt. Soc. Am.* B **13** 1054
[6] Savona V, Andreani L C, Schwendimann P and Quattropani A 1995 *Solid State Commun.* **93** 733
[7] Tanaka T, Zhang Z, Nishioka M and Arakawa Y 1996 *Appl. Phys. Lett.* **69** 887
[8] Fisher T A, Afshar A M, Whittaker D M and Skolnick M S 1996 *Microcavities and Photonic Bandgaps: Physics and Applications* ed J Rarity and C Weisbuch (Dordrecht: Kluwer) p 77
Fisher T A, Afshar A M, Whittaker D M and Skolnick M S 1995 *Phys. Rev.* B **51** 2600
Fisher T A, Afshar A M, Whittaker D M and Skolnick M S 1996 *Phys. Rev.* B **53** R10 469
[9] Nakagawa S, Yamada N, Mikoshibo N and Mars D E 1995 *Appl. Phys. Lett.* **66** 2159
[10] Chen X 1998 *Semicond. Sci. Technol.* **13** 27
[11] Hubner B, Zengerle R and Forchel A 1995 *Appl. Phys. Lett.* **66** 3090
[12] Rarity J and Weisbuch C (ed) 1996 *Microcavities and Photonic Bandgaps: Physics and Applications* (Dordrecht: Kluwer)
Burstein E and Weisbuch C (ed) 1995 *Confined Electrons and Photons* (New York: Plenum)
Yokoyama H and Ujihara K (ed) 1995 *Spontaneous Emission and Laser Oscillation in Microcavities* (Boca Raton, FL: Chemical Rubber Company Press) and references therein
[13] Keller O 1996 *Phys. Rep.* **268** 85
[14] Chen X and Keller O 1997 *Phys. Rev.* B **55** 15 706
[15] Chen X 1997 *Solid State Commun.* **104** 125
[16] Chen X 1997 *J. Phys.: Condens. Matter* **9** 8249
[17] Chen X 1997 *Phys. Scr.* **56** 487
[18] Chen X and Keller O 1997 *Phys. Status Solidi* b **203** 287
[19] Chen X 1998 *Phys. Scr.* at press
[20] Born M and Wolf E 1989 *Principles of Optics* (New York: Pergamon) p 66